ALMA MATER STUDIORUM
UNIVERSITÀ DI BOLOGNA

ARCHIVIO ISTITUZIONALE
DELLA RICERCA

Alma Mater Studiorum Università di Bologna
Archivio istituzionale della ricerca

Linking and link complexity of geometrically constrained pairs of rings

This is the final peer-reviewed author's accepted manuscript (postprint) of the following publication:

Published Version:
Orlandini E., Tesi M.C., Whittington S.G. (2021). Linking and link complexity of geometrically constrained pairs of rings. JOURNAL OF PHYSICS. A, MATHEMATICAL AND THEORETICAL, 54(50), 1-14 [10.1088/1751-8121/ac385a].

Availability:
This version is available at: https://hdl.handle.net/11585/845827 since: 2022-01-16

Published:
DOI: http://doi.org/10.1088/1751-8121/ac385a

Terms of use:

Some rights reserved. The terms and conditions for the reuse of this version of the manuscript are specified in the publishing policy. For all terms of use and more information see the publisher's website.

This item was downloaded from IRIS Università di Bologna (https://cris.unibo.it/).
When citing, please refer to the published version.

(Article begins on next page)

12 October 2024

This is the final peer-reviewed accepted manuscript of:

Orlandini, E., Tesi, M. C., & Whittington, S. G. (2021). Linking and link complexity of geometrically constrained pairs of rings. ***Journal of Physics A: Mathematical and Theoretical, 54*****(50)**

The final published version is available online at ***https://dx.doi.org/10.1088/1751-8121/ac385a***

Terms of use:

Some rights reserved. The terms and conditions for the reuse of this version of the manuscript are specified in the publishing policy. For all terms of use and more information see the publisher's website.

This item was downloaded from IRIS Università di Bologna (https://cris.unibo.it/)

When citing, please refer to the published version.

Linking and link complexity of geometrically constrained pairs of rings

E. Orlandini[1], M. C. Tesi[2] and S. G. Whittington[3]
[1] Dipartimento di Fisica e Astronomia e Sezione INFN, Università di Padova, Via Marzolo 8, I-35131 Padova, Italy
[2] Dipartimento di Matematica, Università di Bologna, Piazza di Porta San Donato 5, I-40126 Bologna, Italy
[3] Department of Chemistry, University of Toronto, Toronto M5S 3H6, Canada

October 14, 2021

Abstract

We investigate and compare the effects of two different constraints on the geometrical properties and linking of pairs of polygons on the simple cubic lattice, using Monte Carlo methods. One constraint is to insist that the centres of mass of the two polygons are less than distance d apart, and the other is to insist that the radius of gyration of the *pair* of polygons is less than R. The second constraint results in links that are quite spherically symmetric, especially at small values of R, while the first constraint gives much less spherically symmetric pairs, prolate at large d and becoming more oblate at smaller d. These effects have an influence on the observed values of the linking probability and link spectrum.

Keywords: Links, lattice polygons, Monte Carlo methods.

1 Introduction

Linking between ring polymers is important if their spatial overlap is not negligible, so one has to consider situations in which the rings are not too far apart. Spatial proximity can be achieved by imposing some geometric constraint on the configuration based for instance on one of its metric properties. The most commonly used consists in partitioning the space of ring pairs with respect to the distance between the two centres of mass, d_{cm} (see Figure 1(a)) . By looking numerically at the linking probability $P_{link}(d_{cm} \leq d)$ as a function of d for lattice and off-lattice models of pairs of rings it was found that, as d decreases the constraint becomes more severe increasing the overlap between the components and hence the probability that they are linked [1, 2, 3].

Little is known rigorously, but by focussing on pairs of unknotted linked polygons in the cubic lattice of the same length n it was found that the number of embeddings grows exponentially with n, with the exponential growth rate being independent of their link type. If instead topologically linked pairs of polygons are constrained to have a pair of edges (one for each polygon) within a fixed distance d their exponential growth rate is equal to that of topologically unlinked ones [2, 4]. Hence, unlike knotting, we cannot say that unlinked pairs are exponentially rare.

Similarly to what was done for knotting [5, 6, 7, 8] one can also look at the linking properties of pairs of rings whose total radius of gyration R_{12} is below a given value R (see Figure 1(b)). As we

shall see later, this constraint should select configurations that are more isotropically organized in space than those based on the distance d_{cm} and closer to those that are confined within a sphere of radius R. As a matter of fact, geometrical confinement is the most natural context where one can address random linking. The first studies along this direction were carried out using both rigorous arguments and numerical simulations on pairs of polygons on the cubic lattice confined into a cube of edge length L [2]. In this case, by using the two-variable Alexander polynomial as a link detector it was found that the linking probability between pairs of polygons, each of n steps, confined in an L-side cube is an increasing function of the scaled variable $n/L^{1/\nu}$ where ν is the metric exponent for self-avoiding walks.

The study of random linking under confinement was later extended to pairs of n edge uniform random polygons confined in a unit cube [9] where it was shown that their linking probability approaches unity at least as $1 - O(1/n)$ while the mean squared linking number grows as n^2 [10]. Linking of rings has been investigated also in slits and channels and its dependence on the degree of confinement was explored both for on and off lattice models [11, 12, 13]. In the case of two n-step polygons confined into tubes and with the additional constraint of sharing the same span s rigorous results based on a pattern theorem in a tube show that their topological linking probability approaches one exponentially fast with either n or s [12].

The linking probability measures the relative number of pairs of rings that are linked irrespective of their link type. Similarly to what has been done for knotted rings under several conditions it is however interesting to look at the topological complexity of the observed links and at its dependence on n, strength of constraint or degree of confinement. With the exception of the study reported in [14] where the complexity of the linked pairs has been explored by looking at the distribution of the linking number, no studies are to our knowledge available either on the link probability or on the population of link types (link spectrum) of pairs of rings subject to different geometrical constraints.

Here we explore this issue for two models of constrained pairs of polygons in the cubic lattice: one in which the constraint is a function of the distance between the centres of mass of the two polygons and the other based on the total radius of gyration of the pair. By performing extensive Monte Carlo simulations on both models we compare the metric and shape properties of the corresponding deformed sampled configurations and show how and to what extent the strength and nature of the constraint affects the linking probability and link complexity of the system.

The plan of the paper is as follows. In Section 2 we introduce the models and give a brief description of the Monte Carlo approach that we use to sample the corresponding constrained configurations at equilibrium. We also present the metric and shape observables and describe the different strategies that we have implemented to detect linking and link type.

In Section 3 we compare the configurational properties of the two models by first looking at their metric and geometrical properties and then focussing on the linking probability and link spectrum.

We close with a short Summary.

2 Models and Methods

In this study ring polymers are modelled as n step lattice polygons, *ie* embeddings of simple closed curves in the simple cubic lattice, Z^3. To sample pairs of such polygons we used the algorithm described in [2] where two-point pivot moves are attempted on either polygon with uniform probability and self and mutual avoidance are checked by standard hash coding procedures.

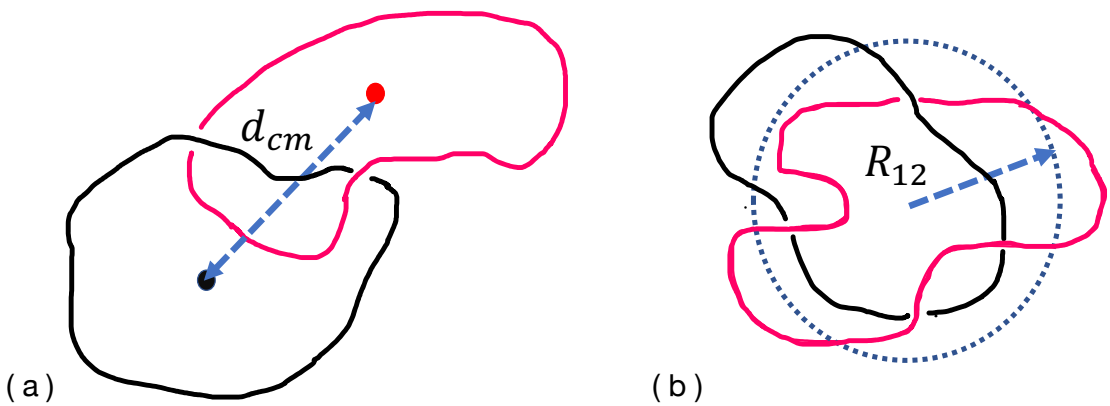

Figure 1: The constraining length $\ell(\mathcal{C})$ used in model d (a) and model R (b).

To keep the polygons reasonably close in space we consider two geometrical constraints, one based on the distance d_{cm} between the two centres of mass and the other on the total radius of gyration of the system, R_{12} (see Figure 1). Let us refer to these two models as *model d* and *model R* respectively. For each configuration (i.e. pair of polygons) $\mathcal{C}$ we associate the length $\ell(\mathcal{C})$ that we use to apply the geometrical constraints for the two models. Specifically, $\ell(\mathcal{C})$ is d_{cm} in model d and R_{12} in model R. Given $\ell(\mathcal{C})$ the idea is to perform an importance sampling procedure i.e. a Monte Carlo sampling with respect to a probability distribution proportional to $\exp(-\beta\ell^2(\mathcal{C}))$.

For given values of n and β, the number of sampled polygon pairs with length ℓ is proportional to the density of configurations $W_n(\ell^2;\beta)$ and to the weight $\exp(-\beta\ell^2)$:

$$N_n(\ell^2;\beta) = W_n(\ell^2;\beta)e^{-\beta\ell^2}. \tag{1}$$

2.1 Multiple Markov chain and multi-histogram reweighting

From a numerical estimate of $N_n(\ell^2;\beta)$ one can get an estimate of $W_n(\ell^2;\beta)$ by performing a reweighting procedure on the sampled configurations. A more robust procedure consists in optimally superimposing the estimates of $W_n(\ell^2;\beta)$ obtained at different values of β and recover the full density of states $W_n(\ell^2)$ for a wide range of values ℓ^2. The optimal superimposition is obtained using the standard Ferrenberg-Swendsen multiple histogram reweighting approach [15] Once $W_n(\ell^2)$ is known (note that its logarithm provides the configurational entropy) the unbiased average of any observable of interest O_n can be estimated as,

$$\langle O_n \rangle = \frac{\sum_{\ell^2} W_n(\ell^2)\bar{O}_n(\ell^2)}{\sum_{\ell^2} W_n(\ell^2)}, \tag{2}$$

where $\bar{O}_n(\ell^2)$ is the average of O_n over the set of configurations $\mathcal{C}$ with $\ell(\mathcal{C})^2 = \ell^2$.

The error in the average 2 is estimated from the semi-dispersion observed by applying the multi-histogram method separately to the first and second halves of the configurations generated by Monte Carlo. Moreover, to decrease significantly the autocorrelation time in the system and hence to perform a more effective sampling of the accessible conformational phase space the multiple Markov chain scheme is also implemented [16, 17].

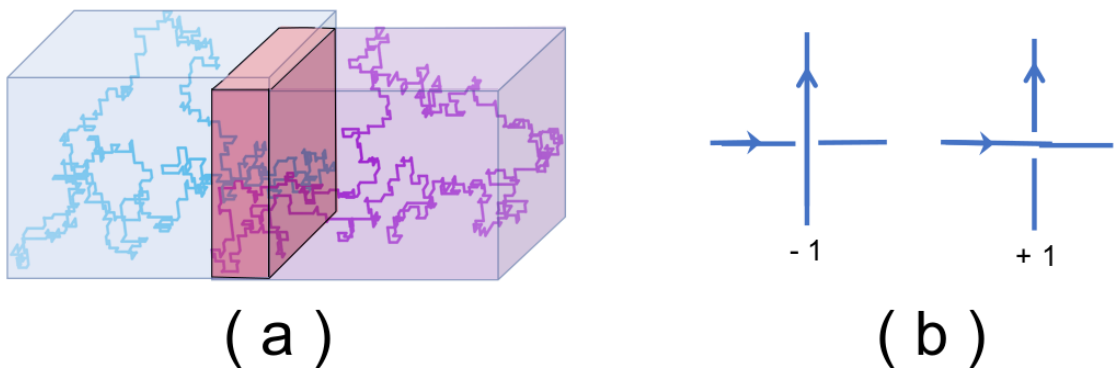

Figure 2: (a) The overlap red box is the intersection between the two spanning boxes of the polygons. (b) Positive and negative crossings determined by the right hand rule.

2.2 Metric properties and degree of overlap

To characterize the geometrical properties of the pairs we compute the radius of gyration (or shape) tensor of each component

$$S_{\alpha\beta} = \frac{1}{2n^2}\sum_{i=1}^{n}\sum_{k=1}^{n}(r_i^\alpha - r_k^\alpha)(r_i^\beta - r_k^\beta), \qquad (\alpha = x, y, z; \beta = x, y, z) \tag{3}$$

where r_i^α denotes the α-coordinate of the i-vertex. Since $S_{\alpha\beta}$ is a real non-negative definite symmetric matrix it has 3 real eigenvalues $\lambda_1 \geq \lambda_2 \geq \lambda_3$ whose square roots measure the semiaxis lengths (a, b, c respectively) of the corresponding ellipsoid (the eigenvectors provide the direction in space of these axes). In particular we look at the squared radius of gyration $R^2 = a^2+b^2+c^2$ that estimates the average extension of the polygons (either one or both components), the asphericity

$$\Delta = \frac{(a-b)^2 + (a-c)^2 + (b-c)^2}{2(a+b+c)^2},$$

a measure of the degree of anisotropy of the system, and the prolateness

$$P = \frac{(2a-b-c)(2b-a-c)(2c-a-b)}{2(a^2+b^2+c^2-ab-ac-bc)^{3/2}}$$

that measures the changeover from oblate to prolate shapes [18]. Δ can range from zero (spherical) to +1 (rodlike) while P can range from -1 (oblate) to +1 (prolate).

A simple way to measure the degree of spatial overlap between the two polygons is to look at the volume of the region shared by them. This is defined as the intersection of the boxes B1 and B2 that contain respectively polygon 1 and 2 (see Figure 2(a)). Denoting by V_o the volume of this box and by V the total volume of the box containing the pair, we consider the overlap volume fraction V_o/V.

2.3 Detecting linking and link type

Let us now describe the different strategies we use to detect and classify the topological state of the mutual entanglement between the two polygons. These are based on the notion of topological links.

Rigorously two disjoint simple closed curves C_1 and C_2 are topologically unlinked (or splittable) if there exist a homeomorphism of $\mathbb{R}^3$ onto itself, $H : \mathbb{R}^3 \to \mathbb{R}^3$, such that the images $H(C_1)$ and $H(C_2)$ can be separated by a plane [19]. Although this is the most general definition of unlinking it not very convenient as link detector especially if one is dealing with a large number of random configurations.

A weaker but more practical notion of linking is based on the computation of the linking number Lk, *homological linking*: one first orients each of the two rings C_1 and C_2 and projects them onto a plane. In general the projection will have mutual crossings and, for almost all projection directions, these will be transverse so that we can assign a value $+1$ or -1 to each crossing according to its orientation (see Figure 2(b)). The sum of these crossing numbers is the linking number of the two curves, $Lk(C_1, C_2)$. This number does not depend on the chosen projection direction and and the two curves are homologically unlinked if and only if $Lk(C1, C2) = 0$ [19]. Since the sign of Lk depends on the orientation attached to the two polygons we consider only its absolute value $|Lk|$. For the Hopf link (the simplest non trivial link) $|Lk| = 1$ while for the $(2, 4)$-torus link, 4_1^2 (known also as the Solomon link,) $|Lk| = 2$. Note that if $|Lk| \neq 0$ the two polygons are topologically linked but $|Lk| = 0$ does not necessarily mean that that the pair is topologically unlinked. For instance the Whitehead link 5_1^2 has $|Lk| = 0$. Moreover, it cannot distinguish between links such as the links 2_1^2 and 6_3^2 ($Lk = 1$) or the links 4_1^2 and 6_2^2 ($Lk = 2$) and so on. On the other hand it provides a coarser description of the topological complexity of all linked configurations including those with minimal crossing number greater than 7.

A more precise detector of topological linking is based on the computation of the two-variable Alexander polynomial [20, 21, 22] $\Delta(t, s)$. This invariant detects some links such the Whitehead link, which would be missed by calculating the linking number. Unfortunately also $\Delta(t, s)$ is not a perfect detector and in principle one should rely on more sophisticated polynomial invariants such as the HOMFLY polynomial. However these invariants are computationally more costly and if we restrict ourselves to detect link types with minimal crossing number ≤ 7 the use of $\Delta(t, s)$ should be sufficient since this distinguishes between all pairs of 2-component links with less than 8 crossings.

The computation of both $\Delta(t, s)$ and $|Lk|$ could be prohibitively costly if the number of crossings n_c after a planar projection is very large. This is indeed a common situation for pairs of polygons with $n > 1000$ and strongly constrained (i.e. β large) where n_c is often larger than 50 or even 100.

To mitigate this problem we first simplify the geometrical entanglement of each pair while keeping its topology unaltered. This is achieved by shrinking stochastically the polygons with the BFACF algorithm [23, 24, 25] simulated at very small step fugacity K. Since the BFCAF moves have the nice property of preserving the topology [26, 27], if K is small enough, the system will often eventually shrink to its minimal length compatible with its link type. Although this is not always true, very often the shrunk configuration, once projected onto a plane, has a small number of crossings, well below 50. This dramatically reduces the time required to compute $\Delta(t, s)$ and $|Lk|$ making the identification of the link type a quite efficient procedure. It is interesting to notice that most of the unlinked pairs that have been detected have, after shrinking, at least one component with $n = 4$. In all these cases the two components are clearly spatially separable and hence topologically unlinked. When this is not the case, we perform 100 random projections of the shrunk configuration, pick one among those with the minimal number of crossings, compute Lk and evaluate $\Delta(t, s)$ at the points $(2, 2)$ $(3, 2)$, $(2, 3)$ and $(3, 3)$. These numerical values are finally compared to those obtained from the explicit polynomial expression of $\Delta(t, s)$ for link types up to 7 crossings (see for instance the Knot Atlas Web page [28])). For the cases in which the Alexander

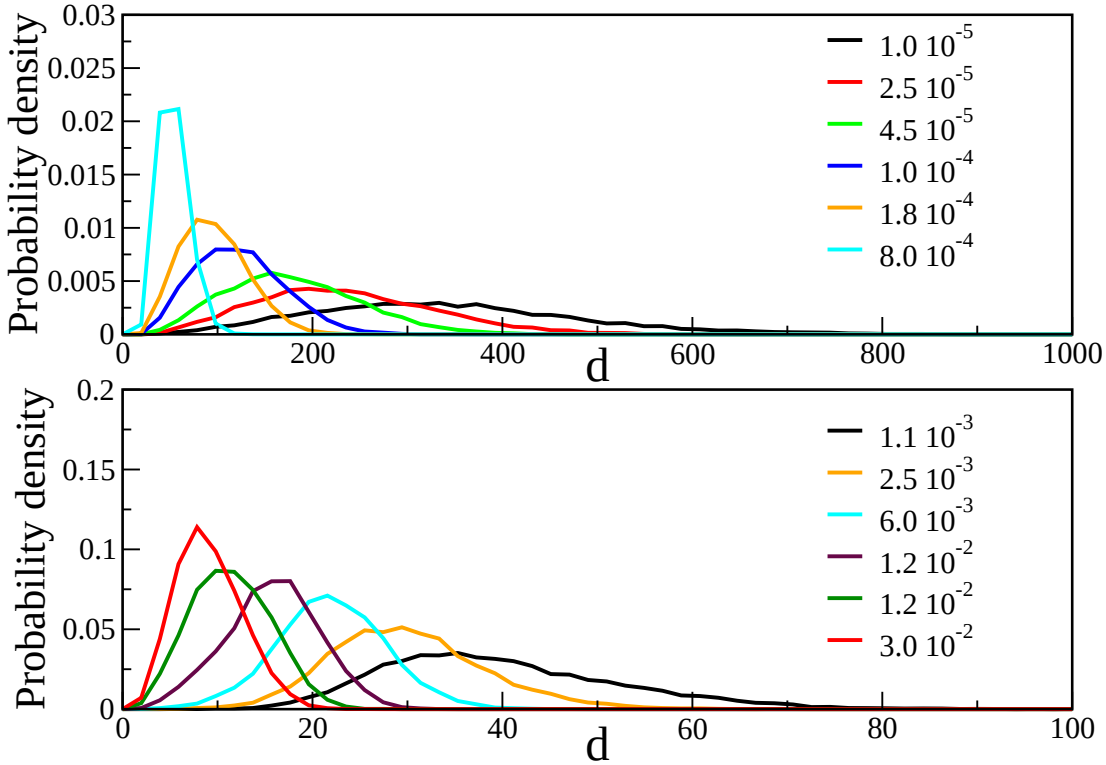

Figure 3: (Color online) Some of the sampled distributions of the distance d_{cm} between centres of mass for different values of β. These refer to the system with polygon length $n = 600$ sampled according to model d.

polynomial is not trivial and no correspondence with links up to 7 minimal crossings is obtained the link is classified as "unknown".

3 Results: comparing the two models

In this section we compare the metric, geometrical and linking properties of the two models described in section 2. The length of polygons considered ranges from $n = 400$ up to 2400 for model d and from $n = 200$ up to 1600 for model R. For each fixed value of n we run an MMC (multiple Markov chain) simulation [16, 17] with up to 27 different values of β chosen such that the probability distributions $\propto \exp(-\beta\ell^2(\mathcal{C}))$ for neighbouring β values have a non-negligible overlap. This will favour a good acceptance rate of swaps between two neighbouring chains. An example of sampled distributions at different values of β is reported for model d in Figure 3. A similar set of distributions can be obtained for model R. For each β we sample $\approx 2 \cdot 10^4$ essentially uncorrelated configurations for a total of at least $5 \cdot 10^5$ samples for each value of n. Examples of equilibrium configurations sampled at intermediate and large value of β are shown in the top row of Figure 4 for polygons with $n = 600$ and geometrically constrained according to model d. By a simple visual inspection one can see that, as β increases, the distance between the two polygons decreases while

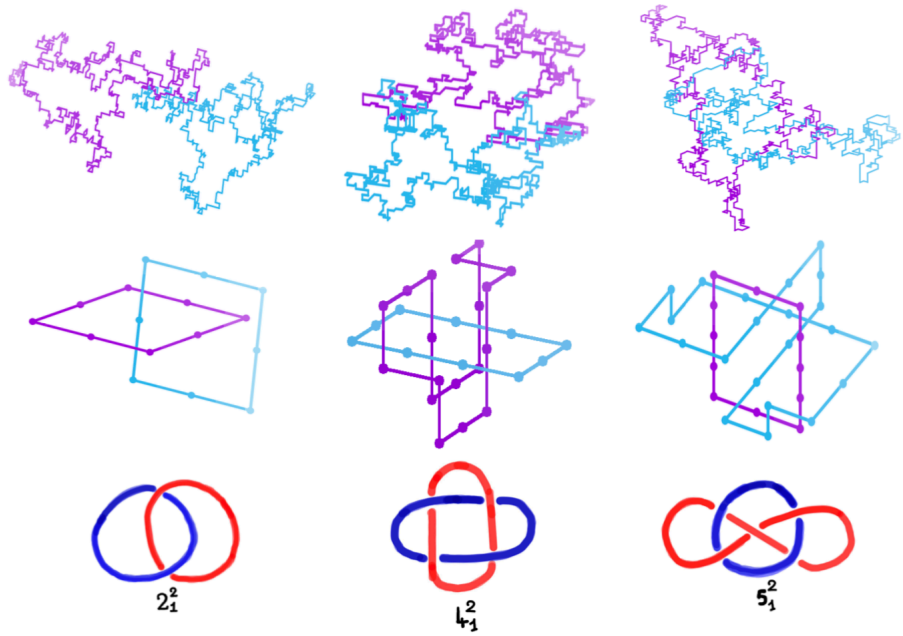

Figure 4: Top row: Pairs of lattice polygons sampled at different values of β ($1.0 \cdot 10^{-5}$ (left), $1.1 \cdot 10^{-3}$ (middle) and $3.0 \cdot 10^{-2}$ (right)) for model d. Their corresponding, topologically equivalent, simplified versions after the smoothing and shrinking procedure via the BFACF algorithm are reported in the middle row while the minimal representation of the associated link type is reported in the bottom row.

their overlap increases. Results for model R are similar.

3.1 Metric and shape properties

In Figure 5(a) and 5(b) we report the average squared radius of gyration of one polygon as a function of the scaled variable $n/\ell^{1/\nu}$, respectively for model d and model R. By using the metric exponent of self-avoiding walks $\nu = 0.5876$ [29] and considering the ratio $\langle R_1^2 \rangle / n^{2\nu}$ the data fall nicely on a single curve, irrespective on the values of ℓ and n. This suggests for both models the following scaling form:

$$\langle R_1^2 \rangle = A(\ell/n^{\nu}) n^{2\nu}. \tag{4}$$

This behaviour is expected since the lengths ℓ and n^{ν} are, for n large enough, the only two relevant length scales of the problem in the swollen phase.

We now focus on the behaviour of the amplitude $A(\ell/n^{\nu})$. For $\ell >> n^{\nu}$ the two polygons are far apart compared to their typical extension and for both models the amplitude is close to 0.1 as expected for unconstrained polygons [30, 31, 32]. For non-negligible constraints, however, the difference between the two models is apparent: in model d the amplitude rapidly increases and then slowly approaches an asymptotic value close to 0.12. This effective swelling of the polygons is the result of the interplay between the constraint that forces their centres of mass to be close

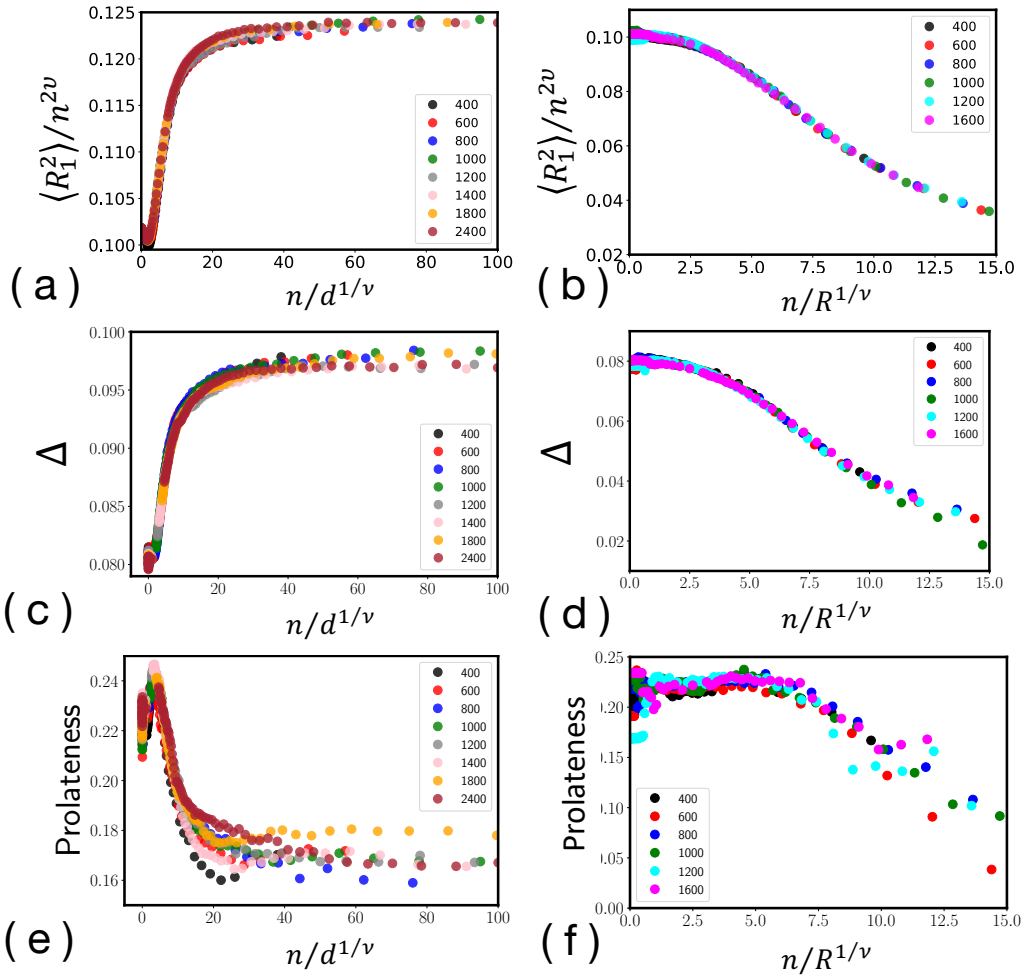

Figure 5: (a,b) Mean squared radius of gyration of a single polygon scaled by $n^{2\nu}$ as a function of the scaled variable $n/\ell^{1/\nu}$ for model d (a) and model R (b). Asphericity Δ and degree of prolateness P for model d (c,e) and model R (d,f). Note that the values of $\Delta \sim 0.08$ and $P \sim 0.24$ found in the uncostrained limit are in agreement with those estimated in [18] for equilateral unknotted and knotted polygons.

and the mutual avoidance that tend to keep them far apart. The net result is the presence of configurations that are more anisotropic than the unconstrained ones. This is confirmed by the behaviour of the asphericity reported in 5(c) whose value increases from its expected value in the bulk $\Delta \sim 0.08$ [18] to 0.1. In model R the function $A(\ell/n^{\nu})$ decreases instead with the strength of the constraint suggesting the sampling of more compact configurations. This is the result of an effective uniform compression of the system due the constraint that in model R depends on the total radius of gyration. This is confirmed by the concomitant decrease of the asphericity from its bulk value to very small values indicating the dominance of configurations with almost spherical shape.

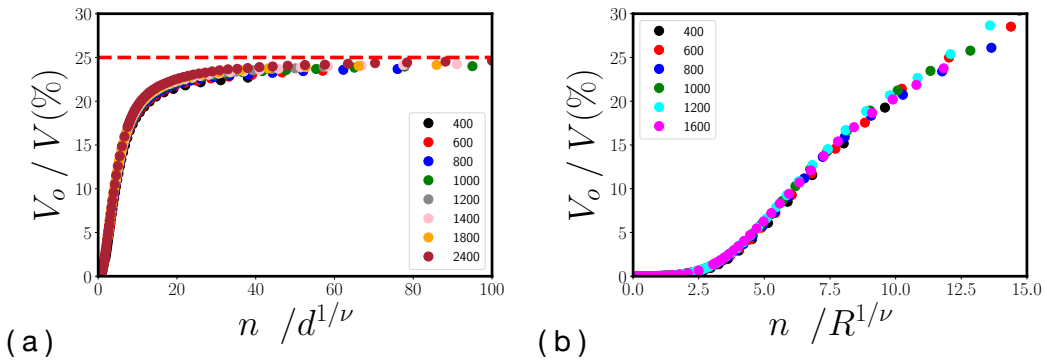

Figure 6: (a,b) Volume fraction of the region shared by both polygons for model d (a) and model R (b). For model d the dashed line corresponds to the case in which 25% of the total volume is shared by the two polygons.

3.2 Overlap and intermingling

The difference between the two models is also apparent in the behaviour of the volume of the overlap region between the two polygons. This is reported in Figure 6(a) and Figure 6(b) for model d and model R respectively. In both models, as the strength of the constraint increases, the overlap volume fraction V_o/V increases. On the other hand, while in model d V_o/V approaches rapidly an asymptotic value $\sim 25\%$, in model R the overlap steadily increases and for the strongest constraint considered is $\sim 30\%$. This suggests that the constraint applied in model R is more effective at forcing the two polygons to overlap.

In summary the isotropic constraint applied in model R provides wider overlap regions and higher degree of intermingling between the two polygons than those provided by the anisotropic constraint of model d that tends to minimize the distance between the centres of mass of the two components. In the next section we shall see how this is reflected in the topological properties (i.e. linking probability and link complexity) of the constrained configurations.

3.3 Linking probability

In Figure 7 we compare our estimates of the topological linking probability P_{link} (i.e. non-trivial Alexander polynomial) of pairs of polygons of the two models. In both cases, similarly to the metric properties, $P_{link}(\ell, n)$ is a function only of the scaling variable $n/\ell^{1/\nu}$. For model d this is in agreement with what was found in [2] for shorter and less asymptotic values of n and d while for model R this is expected from similar results on knots under isotropic confinement [5].

From the behaviour of $P_{link}(n/\ell^{1/\nu})$ one can distinguish three regimes: With a very mild constraint ($\ell >> n^{\nu}$) the two polygons are sufficiently far apart and $P_{link}(n/\ell^{1/\nu})$ is practically zero. As the constraint becomes more severe (i.e. $n/\ell^{1/\nu}$ increases) the two polygons are forced to approach each other, increasing their overlap volume and degree of intermingling (see Figure 6). Consequently this second regime is characterized by a steady increase of $P_{link}(n/\ell^{1/\nu})$.

The difference between the two models is apparent in the strongly constrained regime where the approach of the two polygons to each other competes severely with their mutual avoidance giving rise to different deformed configurations. While in model R this corresponds to an expected change in convexity of P_{link} followed by a very slow growth towards an asymptotic value well above 0.5

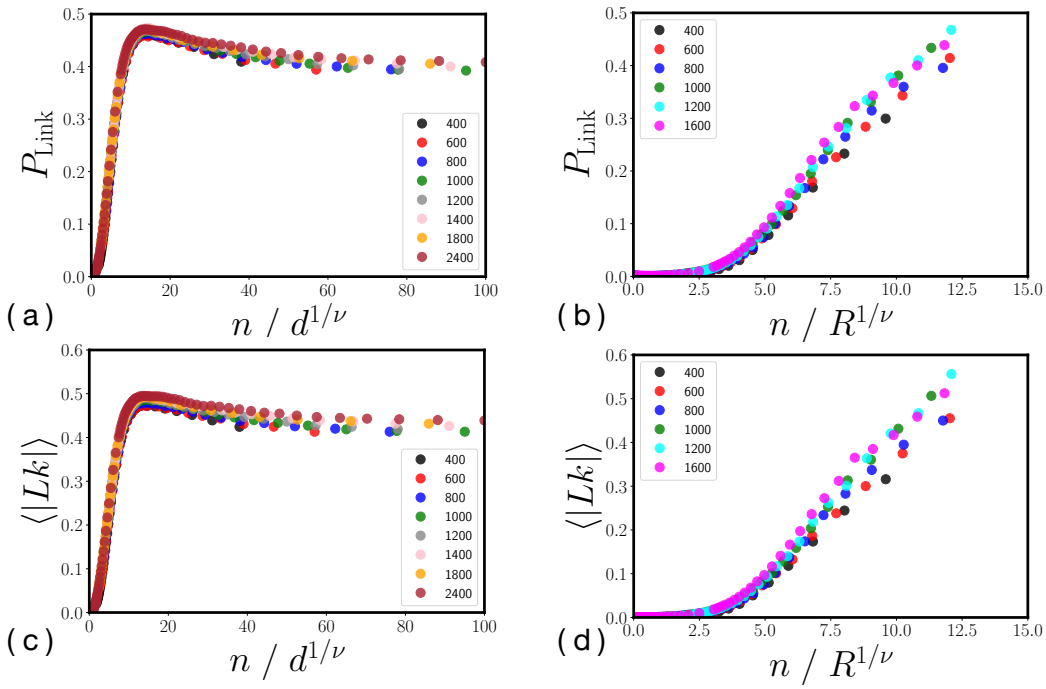

Figure 7: (a,b) Topological linking probability, P_{link} based on the computation of the 2-variables Alexander polynomial for model d (a) and model R (b). (c,d) Average of the absolute value of the linking number for model d (c) and model R (d). As for the metric properties, the data of P_{link} and $\langle |Lk| \rangle$ once plotted with respect to the scaled variable $n/\ell^{1/\nu}$ nicely collapse into a single curve.

(see Figure 7(b)), the behaviour of P_{link} in model d is non-monotonic displaying a maximum value around 0.48 at $n/\ell^{1/\nu} \sim 15$ followed by a mild decrease of P_{link} towards an asymptotic value ~ 0.4 (see Figure 7(a)). Note that this non-monotonic behaviour, that was previously observed for an off-lattice model of pairs of self-avoiding polygons [3], cannot be ruled out by the data shown in [2] for lattice polygons. However in that study the constraint was not sufficiently strong to observe the onset of a maximum and it was natural to conjecture a slow monotonic increase of P_{link} up to an asymptotic value numerically undetermined but clearly well below 1.

Here, given the large number of uncorrelated samples, we are confident that this behaviour is not due to poor statistics in the strongly constrained regime (i.e small values of d). Neither is it likely to be an artifact due to the failure of the link detection procedure based on the Alexander polynomial because the fraction of unknown links is too low ($\sim 0.08\%$, see next section on link spectrum) to affect the observed decrease of P_{link} that is of the order of 10%. Moreover the same behaviour is observed for the average of the absolute value of the linking number (see Figure 7(c)) whose value can be easily computed even for very complex links.

Notice that the decrease of P_{link} is not accompanied by a similar behaviour of the overlap fraction that is practically constant in the strongly constrained regime (see Figure 6(a)). Instead, it is associated with a substantial change in the shape of the linked pair as $n/d^{1/\nu}$ changes, as seen in Figure 5. As d decreases at fixed n the linked pair at first becomes more prolate as the centres of mass become closer together. As d continues to decrease, the prolateness decreases and the pair become more oblate with a concomitant decrease in linking probability.

It is also interesting to compare the linking probability of the two models when plotted as a

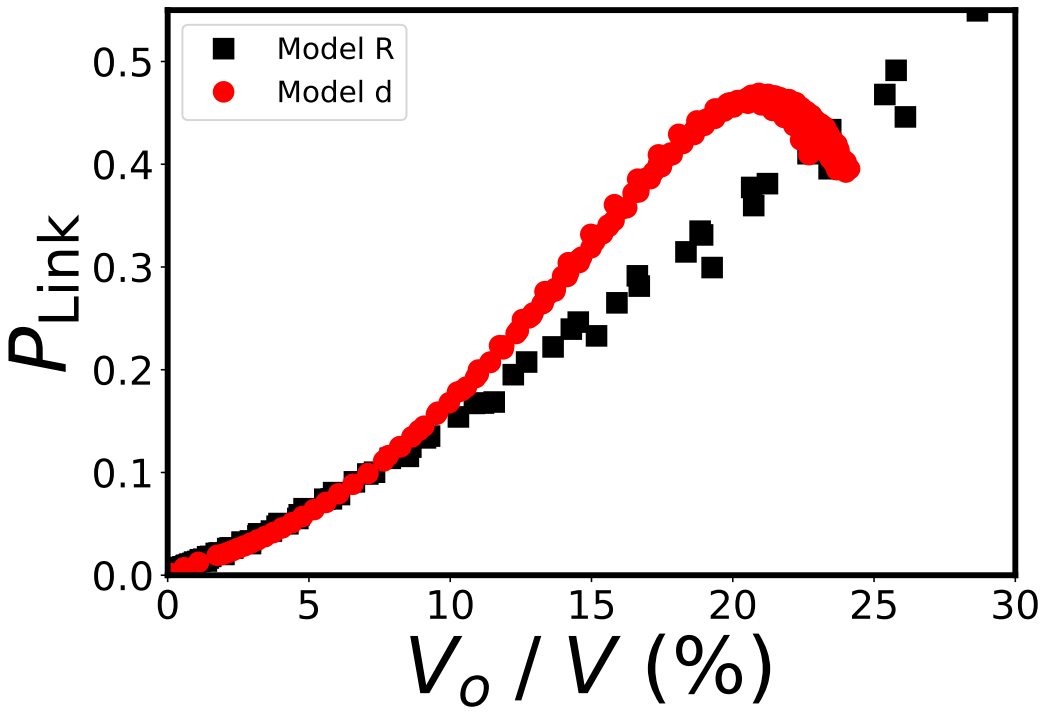

Figure 8: Topological linking probability as a function of the fraction of the volume overlap V_o/V for different values of n. Red circles and black squares refer to model d and model R respectively.

function of the overlap volume fraction. This is reported in Figure 8 for the two models. One can see that, while in the weakly constrained regime (up to 10% of the overlap) the two linking probabilities are equivalent, for sufficiently strong constraints the two curves deviate from one another: while for model d the value of the overlap is slowly saturating and the corresponding linking probability is slightly decreasing, for model R the overlap is still steadily increasing as does the corresponding P_{link} curve. For model R this presumably reflects the continuing tendency to become roughly spherical as the degree of overlap increases.

3.4 Link complexity and link spectrum

The simplest way to look at the link complexity of the sampled configurations is to partition them according to their value of $|Lk|$. As mentioned before this method cannot classify links such as the Whitehead link since for them $|Lk| = 0$. Moreover this classification is rather coarse since there are many link types with the same value of $|Lk|$ [19], but it provides a first estimate of how the link complexity increases with the constraints.

In Figure 9 we compare the probabilities that a given pair of polygons have $|Lk| = 1$ for the two models. The family of links with $|Lk| = 1$ is by far the largest population in both models (i.e. one order of magnitude larger than cases $|Lk| = 2, 3$).

Finally, based on the identification of the values of $\Delta(s, t)$ we perform a finer study of the link complexity by identifying the link type for most of the observed configurations up to 7 crossings. In Table 1 we report the link spectrum of the sampled configurations for pairs of polygons, each of length $n = 1600$, at different values of the constraint strength $n/\ell^{1/\nu}$ for the two models (model

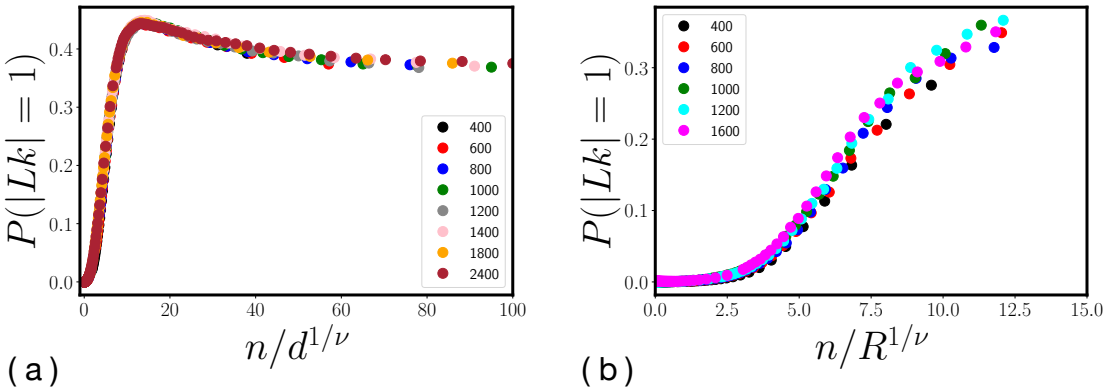

Figure 9: Probability that a given pair of polygons have $|Lk| = 1$ for model d (a) and R (b).

d top table and model R bottom table). For both models, as the strength of the constraint increases, the population of trivial links (or unlinks, 0_1^2) steadily decreases. This is accompanied by a rapid increase of the simplest link in the complexity ladder, the Hopf link (2_1^2) that, for sufficiently strong constraints, reaches a population of $\sim 40\%$ of the whole set of configurations (i.e. unlinks included). As the strength of the constraint increases other links become populated with a ranking that decreases with increased link complexity. It is interesting to notice the relatively high production of two-components links with one knotted (trefoil) component that in model R becomes the third largest population of linked pairs. The presence of a large population of links with knotted components in model R can be again explained by the isotropic compression experienced by both components well below their natural extension in the bulk.

It is also apparent that the geometrical constraint applied in model R gives rise to a rather rich link spectrum where rather complex links (with 6 crossings) have a non-negligible population. As a matter of fact the population of unclassified (UN) links (i.e. with more than 6 crossings) becomes relevant in the largest constraint limit. The unclassified links are either prime 2-component links with large crossing number or the connect sum of a prime 2-component link and a knot.

4 Summary

In this paper we have compared two ways of geometrically constraining pairs of rings in space and have investigated their linking probability and link spectrum as a function of these constraints. The pairs of rings (components of the link) are described as two self and mutual avoiding polygons each of n-steps on the cubic lattice. The two geometrical constraints that we have considered to keep the two components proximal in space are based respectively on the distance between their centres of mass, d_{cm}, (model d) and the total radius of gyration R of the system (model R). The equilibrium configurations have been sampled by Monte Carlo simulations based on two-point pivot moves, importance sampling and MMC scheme. The detection of topological links is based on the computation of the two-variable Alexander polynomial, after a preliminary and crucial geometrical simplification of the configurations based on BFACF moves.

The results that we have obtained can be summarized as follows:

1. From a geometrical point of view, the deformed configurations of the two models differ in

Link type %									
$n/d^{1/\nu}$	0_1^2	2_1^2	4_1^2	5_1^2	6_1^2	6_2^2	6_3^2	$2_1^2\#3_1$	UN
1.18	98.86	1.11	0.02	0.00	0.00	0.00	0.00	0.01	0.00
8.78	57.69	39.91	1.62	0.15	0.02	0.02	0.02	0.53	0.04
14.7	52.95	43.99	2.18	0.18	0.04	0.03	0.02	0.56	0.05
117	59.55	36.89	2.62	0.21	0.09	0.04	0.03	0.52	0.05

Link type %									
$n/R^{1/\nu}$	0_1^2	2_1^2	4_1^2	5_1^2	6_1^2	6_2^2	6_3^2	$2_1^2\#3_1$	UN
1.78	99.59	0.40	0.01	0.00	0.00	0.00	0.00	0.01	0.00
5.59	86.62	12.26	0.53	0.08	0.02	0.00	0.03	0.30	0.15
7.80	71.64	23.87	2.05	0.45	0.09	0.03	0.11	0.98	0.70
10.79	59.98	30.13	4.37	0.99	0.19	0.1	0.38	2.22	1.41

Table 1: Link spectrum for model d (top table) and model R (bottom table) for pairs of polygons each of N=1600 edges and for four values of the scaled variable $n/\ell^{1/\nu}$ quantifying the degree of constraint (first column). From the second to the last column we report the fraction of pairs of polygons with a given link type. The last column (UN) refers to the pairs of polygons with links having more than 6 minimal crossings.

the strongly constrained regime both in their metric and overlap properties. Specifically, the configurations of model d are more anisotropic and display a degree of overlap and intermingling of the two components that saturates in the strong constraint limit. This is clearly the result of bringing the centres of mass of two mutually avoiding rings as close together as is possible. In model R we observe instead more isotropic and spherical configurations that are characterized by higher degrees of overlap and intermingling that, for the degree of compression achieved here, are still increasing.

2. The above properties reflect in the behaviour of the linking probability as a function of the constraint strength. In model d the more anisotropic configurations display a linking probability that, in the strong constraint regime, displays a non-monotonic behaviour with an optimal (maximum) value followed by a slow decrease towards an asymptotic value ~ 0.4. For model R the steady increase of overlap (and intermingling) is accompanied by a monotonic increase of the linking probability whose change of convexity in the large constraint regime suggests the approach to an asymptotic value above 0.5.

3. By looking at the relative population of link types with up to 7 crossings we show that the isotropic constraint of model R gives rise to configurations with a link spectrum that is much richer in complexity the the one observed for model d.

4. A noticeable result is the presence of a relatively large population of two component links with one knotted component (a trefoil). This is true for both models but in model R this finding is much more pronounced. We argue that the significant presence of knotted components in the linked configurations is again the result of the isotropic compression experienced by each component in model R.

References

[1] Frank-Kamenetskii M D, Lukashin A V and Vologodskii A V 1975 *Nature* **258** 398–402

[2] Orlandini E, Janse van Rensburg E J, Tesi M C and Whittington S G 1994 *J. Phys. A: Math. Gen.* **27** 335

[3] Hirayama N, Tsurusaki K and Deguchi T 2009 *J. Phys. A: Math. Theo.* **42** 105001

[4] Soteros C E, Sumners D W and Whittington S G 1999 *Journal of Knot Theory and Its Ramifications* **8** 49–70

[5] Micheletti C, Marenduzzo D, Orlandini E and Sumners D W 2006 *J. Chem. Phys.* **124** 064903

[6] Micheletti C, Marenduzzo D, Orlandini E and Sumners D 2008 *Biophys. J.* **95** 3591–3599

[7] Diao Y, Ernst C, Montemayor A, Rawdon E and Ziegler U 2014 *Comp. Math. Biophys.* **2** 1–19

[8] Ernst C, Rawdon E J and Ziegler U 2021 *J. Phys. A: Math. Theo.* **54** 235202

[9] Arsuaga J, Blackstone T, Diao Y, Karadayi E and Saito M 2007 *J. Phys. A: Math. Theo.* **40** 1925

[10] Panagiotou E, Millett K C and Lambropoulou S 2010 *J. Phys. A: Math. Theo.* **43** 045208

[11] Tesi M C, Janse van Rensburg E J, Orlandini E and Whittington S G 1998 Topological entanglement complexity of polymer chains in confined geometries *Topology and Geometry in Polymer Science* (Springer) pp 135–157

[12] Atapour M, Soteros C E, Ernst C and Whittington S G 2010 *Journal of Knot Theory and Its Ramifications* **19** 27–54

[13] D'Adamo G, Orlandini E and Micheletti C 2017 *Macromol.* **50** 1713–1718

[14] Xiong Z, Han C C and Liao Q 2012 *J. Chem. Phys.* **136** 134902

[15] Ferrenberg A M and Swendsen R H 1988 *Phys. Rev. Lett.* **61** 2635

[16] Geyer C J and Thompson E A 1992 *J. Royal Stat. Soc.: Series B (Methodological)* **54** 657–683

[17] Tesi M C, Janse van Rensburg E J, Orlandini E and Whittington S G 1996 *J. Stat. Phys.* **82** 155–181

[18] Millett K C, Plunkett P, Piatek M, Rawdon E J and Stasiak A 2009 *J. Chem. Phys.* **130** 165104

[19] Rolfsen D 1976 *Knots and Links* (Mathematics Lecture Series 7, Publish or Perish, Inc., Houston, Texas)

[20] Torres G 1953 *Annals of Mathematics* 57–89

[21] Klenin K V, Vologodskii A V, Anshelevich V V, Dykhne A M and Frank-Kamenetskii M D 1988 *J. Biomol. Struct. Dyn.* **5** 1173–1185

[22] Vologodskiĭ A, Lukashin A and Frank-Kamenetskiĭ M 1975 *JETP* **40** 932

[23] de Carvalho C A, Caracciolo S and Fröhlich J 1983 *Nucl. Phys. B* **215** 209–248

[24] de Carvalho C A and Caracciolo S 1983 *J. Physique* **44** 323–331

[25] Berg B and Foester D 1981 *Phys. Lett. B* **106** 323–326

[26] Janse van Rensburg E J and Whittington S G 1991 *J. Phys. A: Math. Gen.* **24** 5553–5567

[27] Bonato A, Orlandini E and Whittington S G 2020 *J. Phys. A: Math. Theo.* **53** 385002

[28] The Knot Atlas http://katlas.org/wiki/Main_Page

[29] Clisby N 2010 *Phys. Rev. Lett.* **104** 055702

[30] Janse van Rensburg E J and Whittington S G 1991 *J. Phys. A: Math. Gen.* **24** 3935

[31] Quake S R 1995 *Phys. Rev. E* **52** 1176

[32] Orlandini E, Tesi M C, Janse van Rensburg E J and Whittington S G 1998 *J. Phys. A: Math. Gen.* **31** 5953